Available online at www.sciencedirect.com
ScienceDirect
International Journal of Thermal Sciences 47 (2008) 1169–1183
International Journal of Thermal Sciences
www.elsevier.com/locate/ijts

Semi-analytical approach to boiling heat fluxes calculation in subsurface horizontal and vertical tunnels

Robert Pastuszko *, Mieczyslaw E. Poniewski

Chair of Thermodynamics and Fluids Mechanics, Kielce University of Technology, Al. Tysiaclecia P.P. 7, 25-314 Kielce, Poland

Received 23 November 2006; received in revised form 28 September 2007; accepted 2 October 2007

Available online 19 November 2007

Abstract

The paper focuses on theoretical and experimental studies of boiling heat transfer on double-extended surfaces with tunnel structures, covered with perforated foil. The experiments were conducted for water and R-123 at atmospheric pressure. The tunnel external covers were manufactured from perforated copper foil of 0.05 mm in thickness (pore diameters: 0.3, 0.4, 0.5 mm), sintered with the mini-fins, formed on the vertical side of rectangular fins and horizontal inter-fin surfaces. On the basis of their previous studies and existing analytical boiling models, the authors proposed their own model for extended surfaces with connected horizontal and vertical tunnels. Extended surface nonisothermality and the characteristic process of vapor bubbles formation and departure were accounted for. Regarding the calculated bubbles parameters (diameter, nucleation sites density, generation frequency), the heat fluxes for evaporation within the tunnels and convection on the tunnel external surfaces were determined. Substantial enhancement of the heat transfer coefficient was observed for the investigated structures. Calculations, based on the developed simplified model, indicated a predominating convection heat contribution to the heat transfer for tunnel structures. The predicted heat fluxes, when compared to the experimental results, showed satisfying agreement in low and medium heat flux ranges for water, and in all heat flux ranges for R-123.

Keywords: Pool boiling; Subsurface structure; Tunnel structure; Modeling

1. Introduction

The paper deals with a theoretical analysis of boiling heat transfer on extended finned surfaces with additional mini-fins, covered with perforated foil. These are double extended surfaces with joined horizontal and vertical tunnels which, for certain heat flux ranges and some boiling agents, have heat transfer coefficients comparable with commercial structures, Fig. 1.

The subsurface tunnels formed lateral surfaces on the fins and horizontal spaces between main fins (Fig. 1), producing regions of intensive vapor bubble generation. The enhanced structures made use of three passive techniques of boiling heat transfer enhancement:

(1) surface extension—mini-fins and main fins increased in the effective heat transfer area;
(2) perforated foil—permeable pores equilibrate the liquid inflow, evaporation and vapor outflow;
(3) subsurface tunnels, confined spaces—regions of intensive vapor bubble generation.

There were only few studies on the modeling of boiling from tunnel coverings.

Most models for these coverings were based on the concept proposed by Nakayama et al., developed for surfaces of *Thermoexcel* type [1]. Their basic assumptions were the following:

(a) the temperature of the whole liquid volume corresponds to the pressure in the system,
(b) the tunnel wall temperature is constant,
(c) vapor in tunnels and bubbles is in the saturated state,
(d) tunnels are filled with vapor, except for corners with menisci.

* Corresponding author.
E-mail addresses: tmprp@tu.kielce.pl (R. Pastuszko), tmpmp@tu.kielce.pl (M.E. Poniewski).

1290-0729/$ – see front matter
doi:10.1016/j.ijthermalsci.2007.10.003

Nomenclature

A	constant in dependence $\alpha = A\Theta^n$
Bo	Bond number
C_{conv}	convection term
C_{Ham}	Hamaker's constant ..... J
C_{tg}	Chien–Webb constant used for model of growth period
c	constant in Haider–Webb dependence for C_{conv}
c_p	specific heat at constant pressure ..... J/kg K
d	diameter ..... m
f	frequency ..... Hz
g	acceleration due to gravity ..... m/s^2
h	height ..... m
i_{lv}	latent heat of vaporization ..... J/kg
k	exponent in dependence for C_{conv}
l	exponent in Haider–Webb dependence for C_{conv}
m	mass ..... kg
m_f	fin parameter ..... m^{-1}
N	number of pores
n	exponent in dependence $\alpha = A\Theta^n$
n_s	nucleation site density ..... m^{-2}
p	pressure ..... Pa
p_p	pore pitch ..... m
p_{tun}	tunnel pitch ..... m
Pr	Prandtl number
$\dot{Q}$	heat transfer rate ..... W
q	heat flux ..... W/m^2
$\mathbf{R}$	particular gas constant ..... J/kg K
R	bubble radius ..... m
r	radius of meniscus ..... m
s	gap between fins ..... m
T	temperature ..... K
t	time ..... s
TS	tunnel structure
V	volume ..... m^3
w	width ..... m
y	vertical coordinate ..... m

Greek symbols

α	heat transfer coefficient ..... W/m^2 K
δ	thickness ..... m
Δ	difference
ΔT	temperature superheat ($\Delta T = T_{\text{bs}} - T_{\text{sat}}$) ..... K
Θ	local fin superheat ..... K
λ	thermal conductivity ..... W/m K
ρ	density ..... kg/m^3
σ	surface tension ..... N/m

Subscripts

a	active
b	departing bubble
bs	main fin base = horizontal foil level
Cu	structure material (copper)
ex	external
f	fin
H	horizontal
h	hydraulic
i	intake
l	liquid
m	mean
max	maximum
ne	non-evaporating
p	pore
sat	saturation
t	triangular
tip	main fin tip
tun	tunnel
V	vertical
v	vapor
0	beginning of the waiting period
1	beginning of the growth period
2	beginning of the intake period
0–1	waiting period
1–2	growth period
0–2	waiting and growth periods

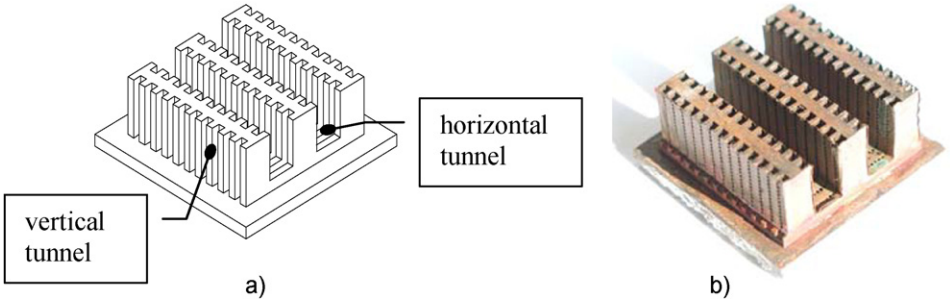

Fig. 1. a) TS sample before being overlaid with perforated foil, b) a photograph of TS sample with the sintered layer of perforated foil.

The authors suggested the possibility of extending their model over a class of coverings with a relatively large volume of interconnected cavities and narrow outlets on the coverings. It is the case for the investigated structure of this study. The suction–evaporation boiling cycle, divided into three phases: *pressure build-up phase*, *pressure reduction phase* and *liquid*

intake phase, was applied to the quoted model. The liquid suction into the tunnels through inactive pores, fostered by the pumping feature of bubbles departing from active pores, was assumed. The liquid propagated along the tunnels and evaporated from the menisci in the corners. This semi-analytical model had six empirical constants. Some experimental data for water, R-11 and nitrogen show the deviation of 300% from the computed values.

The Haider and Webb [2] model envisioned that transient micro-convection in the wake of the departing bubbles was the dominant heat transfer mechanism. Their model was developed for predicting heat flux as a function of nucleation site density, a bubble departure diameter and bubble frequency for plain surfaces with R-11 and R-123 as boiling fluids. Extending the model of Mikic and Rohsenow [3], they created the asymptotic correlation with transient heat conduction to the layer around boiling sites as the main mechanism of nucleate boiling heat transfer. The model could be applied to calculate total heat flux of the enhanced surfaces by adding the latent and external heat fluxes. It showed that the contribution of micro-convection was large compared to transient conduction.

Chien and Webb [4] analytical considerations, developed out of Nakayama's et al. model, were preceded by comprehensive experimental investigations into the influence of geometrical parameters of specially prepared porous structures on boiling heat transfer. It was noticed that the tunnels were fully filled with vapor except for the liquid in the corners, which created menisci. The dynamics of bubble growth while departing from the porous surface was also observed. On the basis of these results they proposed a semi-analytical model for heat transfer in nucleate boiling in a porous structure with subsurface tunnels. The basic quantity determined in this model is the instantaneous evaporation rate inside the tunnel, which is obtained through analyzing the meniscus size, bubble growth, a bubble departure diameter and unsteady convection on the external surfaces of the tunnels. The model used two empirical constants and predicted most boiling heat transfer data for four refrigerants (R-11, R-123, R-134a, R-22) within ±33% tolerance. Two of the above quoted studies [1,4] validated their models for a quite narrow range of wall superheats (below 4 K).

The aim of Ramaswamy et al. [5] was to present a semi-analytical model predicting the bubble departure diameter, frequency, and nucleation site density for boiling enhancement structures. Their enhanced structures had pores of 0.05–0.3 mm in diameter, at pitches with the range of 0.15–0.4 mm. The two previously discussed models by [1] and [4] were used as a framework. Certain simplifications were applied, for instance: linear variation of vapor density and volume with time. Heat flux for FC-72 was predicted with ±50% accuracy. The model's advantage, in comparison to the previous ones, lies in the prediction of the bubble dynamics for a wider range of wall superheats (up to 20 K). Four more experimental constants, compared to the Chien–Webb model, were introduced in order to determine the constant in the equation for external heat flux.

Based on their own visualization studies [6–8] and existing analytical boiling models, Pastuszko and Poniewski [9] proposed their own approach to pool boiling of water in connected horizontal and vertical tunnels.

In the present semi-analytical approach, based on the authors' earliest model, described above, the mechanisms of liquid evaporation in tunnel corners and vapor bubbles cycle were accounted for, as well as the nonisothermality of the main fin, i.e. one-dimensional temperature distribution along vertical tunnels walls. The model was used to determine bubble diameters, nucleation sites density, generation frequency, the evaporation heat fluxes within the tunnels, and heat fluxes on the external surfaces.

2. Enhanced structures

The enhanced structures views, before and after perforated foil sintering, are shown in Fig. 1. Samples with the tunnel structure (TS) formed a square of 27 mm side. They had three main fins with additional surface modification for TS (mini-fins formed by cutting grooves). The constant parameters were as follows, Fig. 2: fin number: 3, main fin height (h_f): 10 mm, fin thickness (δ_f): 5 mm, fin width (w_f): 27 mm, space between fins (s): 5 mm, tunnel height (h_{tun}): 1.6 mm, tunnel width (w_{tun}): 1.3 mm.

The vertical tunnel height was equal to the main fin height and the horizontal tunnel length was equal to the distance between main fins. Grooves were cut on fins lateral (vertical) surface and horizontal inter-fin spaces, copper perforated foil of 0.05 mm in thickness was sintered to the machined surfaces, Figs. 1, 2, 3.

The tunnel dimensions were shown in Fig. 2 and in Table 1—the parameters of the investigated structure with the notations as in Fig. 2.

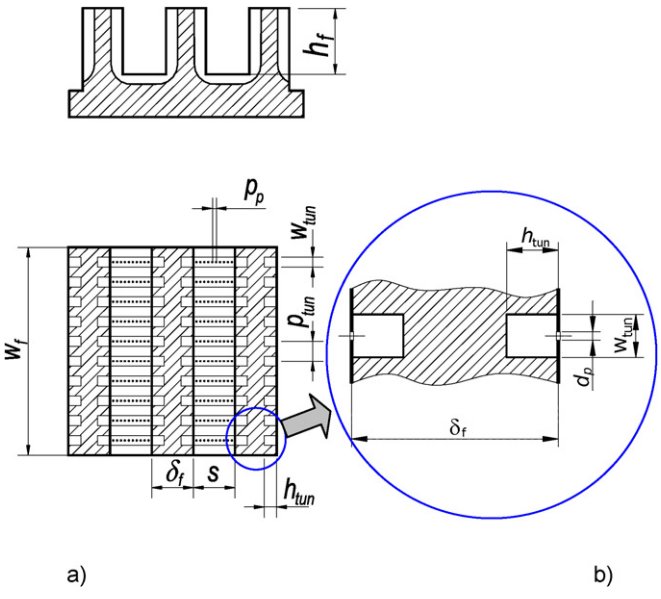

Fig. 2. a) Vertical and horizontal section of the sample with TS. b) Tunnel dimensions (horizontal cross-section of the main fin).

3. Model formulation

3.1. Limitations

The main obstacle in transferring the discussed models into the case of tunnel surfaces with vertical fins covered with perforated foil is the fact that in tunnel structures on finned surfaces three types of boiling may occur simultaneously, due to non-isothermality of the main fin surfaces, and at high wall superheats. Those are thin film evaporation, transition and nucleate boiling, all at adjacent locations from fin base to fin tip respectively. One can calculate the heat flux focusing exclusively on nucleate boiling, which occurs in the widest heat flux range.

3.2. Assumptions

The following boiling mechanism was assumed:

Table 1
Samples code and specifications (dimensions in millimeters)

Sample code	Pore dia. d_p	Pore pitch p_p	Tunnel pitch p_{tun}
TS-10-2.00-0.3	0.3	0.6	2.00
TS-10-2.00-0.4	0.4	0.8	2.00
TS-10-2.00-0.5	0.5	1.0	2.00
TS-10-2.25-0.3	0.3	0.6	2.25
TS-10-2.25-0.4	0.4	0.8	2.25
TS-10-2.25-0.5	0.5	1.0	2.25
TS-10-2.50-0.3	0.3	0.6	2.50
TS-10-2.50-0.4	0.4	0.8	2.50
TS-10-2.50-0.5	0.5	1.0	2.50

(1) The holes in the foil act as elements feeding the surface tunnel structure. The liquid propagates along the tunnels, and the evaporation takes place from menisci in four corners of tunnels with rectangular cross-section (Figs. 3, 4).
(2) The inside of the vertical and horizontal tunnel is filled with vapor, except for a thin film of liquid at the walls and in menisci. Suction and evaporation take place independently for the vertical and the horizontal tunnel, Fig. 3.
(3) The visualization described in [6–8] shows that the bubble release points, that is the points where the vapor generated in menisci in tunnel corners, Fig. 3, flows out, are the following:
   - channels outlet in vertical tunnels,
   - holes in foil (pores)—for horizontal tunnels.
(4) The liquid inflow (suction) to both vertical and horizontal tunnels takes place through the foil pores (Fig. 3).
(5) In the horizontal tunnel, some of the pores (inactive) supply the subsurface area with liquid; some (active) act as vapor outlets and bubble growth points.
(6) Heat transfer is enhanced by the detaching bubbles, mixing the boiling liquid.
(7) The whole process of a bubble formation takes place during one cycle (Fig. 4). Due to the vapor being carried away outside through the detaching bubbles, the liquid is sucked into the tunnels.
(8) The total heat flux, calculated independently for the horizontal and the vertical tunnels, is composed of two parts:
   - evaporation (latent) heat flux, which originates in the liquid layer evaporating inside channels,
   - heat flux transferred by convection above the external surface of the covering.

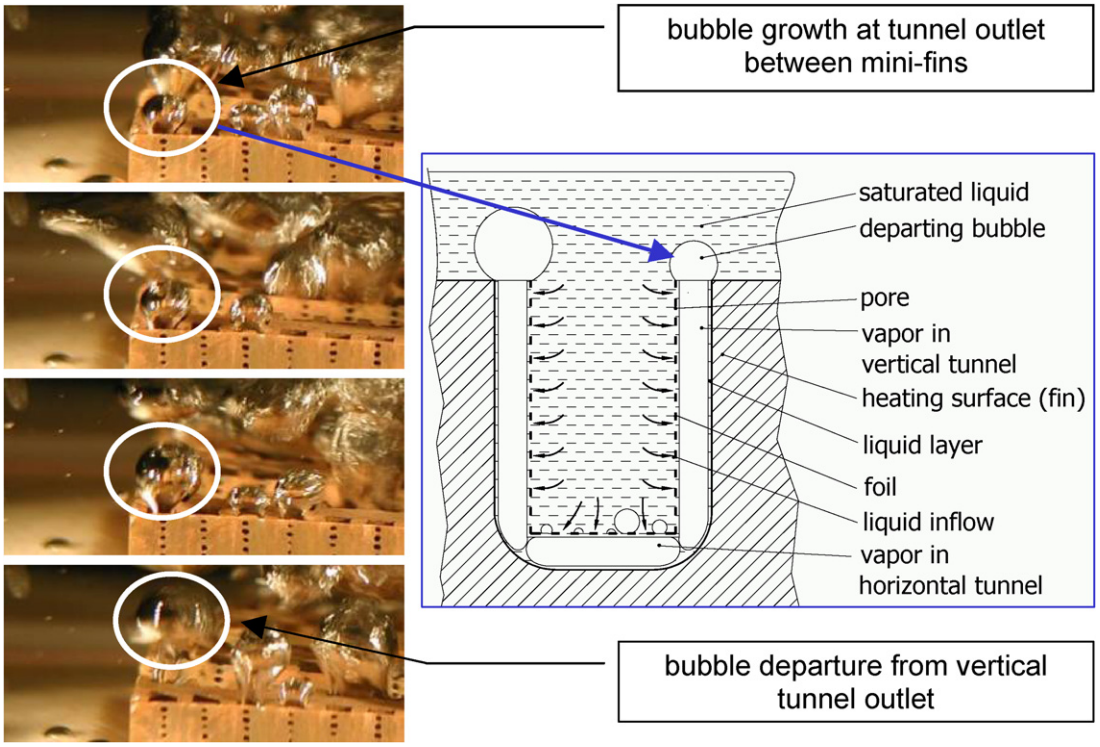

Fig. 3. Left-hand side: bubble growing and departing at vertical tunnel outlet, water, sample TS-10-2.00-0.3; right-hand side: joined tunnels vertical cross-section [8].

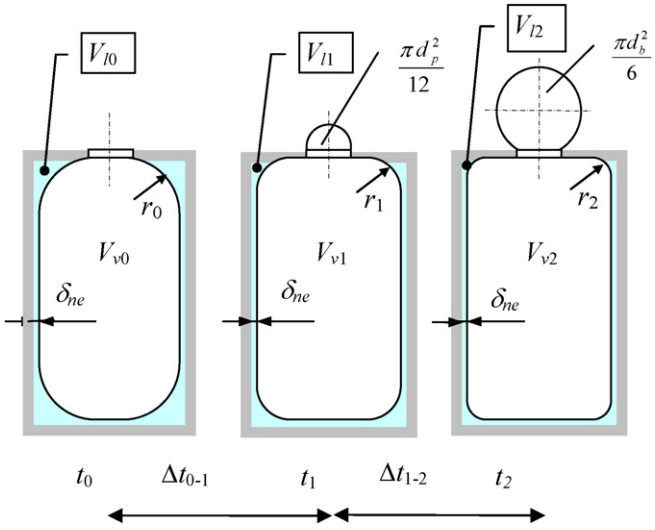

Fig. 4. Liquid evaporation in a horizontal tunnel; bubble growth (Δt_{0-1}—waiting period, Δt_{1-2}—growth period).

(9) Each bubble cycle for both tunnels consists of a waiting period (Δt_{0-1}), a growth period (Δt_{1-2}) and a liquid intake period (Δt_i)—Fig. 4. The last period, much shorter than the other two, was neglected in the calculation of the bubble frequency [1,2,4,5].

(10) In order to take into account the temperature changes occurring on vertical main fins, and simultaneously on the vertical tunnels walls, the heat transfer coefficient along the fins height was assumed to be variable and the mean heat transfer coefficient was determined. The mean heat transfer coefficient and mean parameter m_f were used in order to avoid numerical and complicated analytical solutions to the heat conduction equation. It was also assumed that the same temperature occurs both on the horizontal tunnels walls and at the main fins base.

4. Horizontal tunnel modeling

4.1. Vapor density

Taking into consideration the fact that at the end of the waiting period, that is, at the moment of generating a semi-spherical vapor area, with the diameter equal to the pore diameter, the pressure inside the tunnel is the same as the vapor pressure in the pore section and equals:

$$p_{v1} = p_{\text{sat}} + \frac{4\sigma}{d_p} \tag{1}$$

Using the Clausius–Clapeyron equation in the following form:

$$\frac{\mathrm{d}p}{\mathrm{d}T} = \frac{i_{lv}}{T_{\text{sat}}(\rho_v^{-1} - \rho_l^{-1})} \tag{2}$$

as well as the equation of state of ideal gas, we can express vapor density at the end of the waiting period as:

$$\rho_{v1} = \frac{\rho_{v\text{sat}} + \frac{4\sigma}{\mathbf{R}d_p T_{\text{sat}}}}{1 + \frac{4\sigma}{d_p i_{lv}}(\rho_{v\text{sat}}^{-1} - \rho_l^{-1})} \tag{3}$$

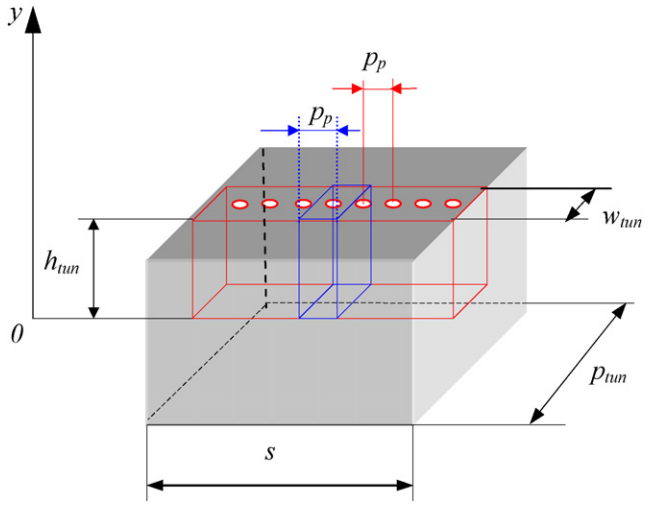

Fig. 5. A horizontal tunnel referred to the pitch segment volume.

The error in the saturated vapor density calculation from the ideal gas state equation was about 2% (for $T_{\text{sat}} = 100\,^{\circ}\text{C}$, $p_{\text{sat}} = 101$ kPa, $\mathbf{R} = 462$ J/kg K).

4.2. Liquid volumes during the waiting and growth periods

Due to lack of inflow and outflow of liquid and vapor for the considered segment (Fig. 5), the increase in vapor volume in the period of waiting and growth is compensated through the decrease in the saturated liquid mass:

$$\mathrm{d}m_v = \mathrm{d}m_l \tag{4}$$

After the introduction of the mean values of vapor volume and density, the change in the vapor mass is given by:

$$\mathrm{d}m_v = V_{vm}\,\mathrm{d}\rho_v + \rho_{vm}\,\mathrm{d}V_v \tag{5}$$

The linear increase of vapor volume during the waiting period was also proved analytically by Ramaswamy et al. and Chen et al. [5,10].

Dividing Eq. (5) by liquid density and taking into account Eq. (4), one obtains the volume of liquid that evaporated during the given period. Assuming linear changes in density and volume, we get the following expression:

$$\Delta V_l = V_{vm}\frac{\Delta\rho_v}{\rho_l} + \Delta V_v \frac{\rho_{vm}}{\rho_l} \tag{6}$$

As shown in Fig. 4, the change in vapor volume during the waiting period is approximately equal to the volume of the generated vapor bubble, i.e. $\pi d_p^3/12$. The total vapor volume change in the waiting period (0–1) and growth period (1–2) will reach volume $\pi d_b^3/6$, where d_b is the departing bubble diameter. The initial vapor volume was compared to the tunnel volume, i.e., $V_{\text{tun}\,H} = w_{\text{tun}} h_{\text{tun}} p_p$, where all volume changes in a horizontal tunnel were considered for the segment of the length equal to pore pitch—p_p, Fig. 5. These considerations refer to the segment with an active pore, that is, a pore in which a vapor bubble is formed with the liquid evaporating in the tunnel menisci. The additional assumptions for the computation of the evaporated liquid volume were as follows:

- mean vapor volume (V_{vm}) during the waiting period is equal to $(V_{\mathrm{tun}\,H} + V_{\mathrm{tun}\,H} + \pi d_p^3/12)/2$ and mean density is $(\rho_{v\,\mathrm{sat}} + \rho_{v1})/2$,
- mean vapor volume (V_{vm}) during the waiting and the growth periods is equal to $(V_{\mathrm{tun}\,H} + V_{\mathrm{tun}\,H} + \pi d_b^3/6)/2$ and mean density is $(\rho_{v\,\mathrm{sat}} + \rho_{v2})/2$.

The volumes of the evaporated liquid in waiting period (0–1) and waiting and growth periods (0–2) respectively, according to Eq. (6), were the following:

$$\Delta V_{l\,0\text{–}1\,H} = \frac{2V_{\mathrm{tun}\,H} + \frac{\pi d_p^3}{12}}{2}\frac{\rho_{v1} - \rho_{v\,\mathrm{sat}}}{\rho_l} + \frac{\pi d_p^3}{12}\frac{\rho_{v\,\mathrm{sat}} + \rho_{v1}}{2\rho_l} \tag{7}$$

$$\Delta V_{l\,0\text{–}2\,H} = \frac{2V_{\mathrm{tun}\,H} + \frac{\pi d_b^3}{6}}{2}\frac{\rho_{v2} - \rho_{v\,\mathrm{sat}}}{\rho_l} + \frac{\pi d_b^3}{6}\frac{\rho_{v\,\mathrm{sat}} + \rho_{v2}}{2\rho_l} \tag{8}$$

Vapor density at the end of growth period, ρ_{v2}, was calculated according to Eq. (3) substituting d_b for d_p. Assuming spherical bubble shape, we adopted the dependence for bubble departure diameter d_b after [4], where it was determined on the basis of geometrical analysis and balance between buoyancy and surface tension forces:

$$d_{b\,H} = \left(\frac{Bo + \sqrt{Bo^2 + 2304(96/Bo - 3)}}{192 - 6Bo}\right)^{1/2} d_p \tag{9}$$

where the Bond number equals $Bo = [d_p^2(\rho_l - \rho_v)g]/\sigma$.

The calculation of the initial volume was made based on the mass conservation equation for times $t = t_0$ and $t = t_2$, that is, for the beginning of the waiting period and the end of the growth period:

$$m_{v0\,H} + m_{l0\,H} = m_{v2\,H} + m_{l2\,H} \tag{10}$$

It is equivalent to:

$$V_{v0\,H}\rho_{v\,\mathrm{sat}} + V_{l0\,H}\rho_l = V_{v2\,H}\rho_{v2} + V_{l2\,H}\rho_l \tag{11}$$

Adopting accurate dependencies for the initial and final vapor volume in the tunnel, i.e. $V_{v0} = V_{\mathrm{tun}} - V_{l0}$, $V_{v2} = V_{\mathrm{tun}} - V_{l2} + \pi d_b^3/6$ and $V_{l2} = V_{l0} - \Delta V_{l0\text{–}2}$, Fig. 4, one gets:

$$(V_{\mathrm{tun}\,H} - V_{l0\,H})\rho_{v\,\mathrm{sat}} + V_{l0\,H}\rho_l = \left[V_{\mathrm{tun}\,H} - (V_{l0\,H} - \Delta V_{l\,0\text{–}2\,H}) + \frac{\pi d_b^3}{6}\right]\rho_{v2} + (V_{l0\,H} - \Delta V_{l\,0\text{–}2\,H})\rho_l \tag{12}$$

After the rearrangement of Eq. (12), the following dependence for initial liquid volume in menisci of the horizontal tunnel was obtained:

$$V_{l0\,H} = \frac{\rho_{v2}(V_{\mathrm{tun}\,H} + \frac{\pi d_b^3}{6}) - (\rho_l - \rho_{v2})\Delta V_{l\,0\text{–}2\,H} - \rho_{v\,\mathrm{sat}}V_{\mathrm{tun}\,H}}{\rho_{v2} - \rho_{v\,\mathrm{sat}}} \tag{13}$$

The liquid volume at the end of the growth period is equal to the difference of the volumes given by Eqs. (13) and (8):

$$V_{l2\,H} = V_{l0\,H} - \Delta V_{l\,0\text{–}2\,H} \tag{14}$$

4.3. Tunnel heat transfer

Due to complexity of the calculation procedure presented in the quoted papers and used for determining meniscus thickness and heat flux in menisci, authors decided to implement some simplifications without significant influence on the accuracy of the heat flux in a horizontal tunnel calculation. On the basis of the geometrical dependencies, Figs. 4, 5, 6, it is possible to calculate radiuses of the menisci at the beginning of the waiting period and at the end of the growth period. The difference between the computed values in the considered approach does not exceed 0.2% and the dependence for the mean radius can be expressed as:

$$r_{m\,0\text{–}2\,H} = \sqrt{\frac{(V_{l0\,H} + V_{l2\,H})/2}{(4 - \pi)p_p}} \tag{15}$$

In order to calculate the heat flux in the meniscus of the active segments, its real cross-section was replaced by a triangular section [9], Fig. 6. Its height was determined from a mean liquid volume in the period 0–2:

$$\delta_{t\,0\text{–}2\,H} = \sqrt{\frac{V_{l0\,H} + V_{l2\,H}}{8p_p}} \tag{16}$$

When we assume one-dimensional heat conduction in the liquid, and temperature superheat ΔT referred to the main fin base, that is, to the elevation of horizontal perforated foil ($y = h_{\mathrm{tun}}$, Fig. 5), the integration of the equivalent area within $\delta_{\mathrm{ne}}\sqrt{2}$ to $\delta_{\mathrm{ne}}\sqrt{2} + \delta_{t\,0\text{–}2\,H}$, Fig. 6, results in the dependence for the latent heat transfer rate from four menisci of the horizontal tunnel:

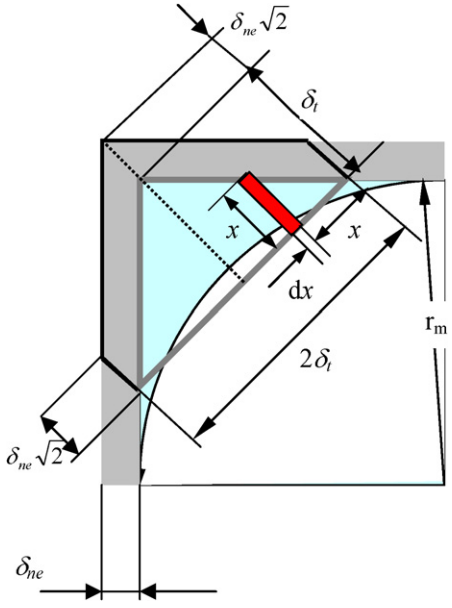

Fig. 6. Defining the equivalent meniscus section.

$$\dot{Q}_{0-2H} = 4 \int_{\delta_{ne}\sqrt{2}}^{\delta_{t\,0-2H}+\delta_{ne}\sqrt{2}} 2\frac{\lambda_l \Delta T}{x} p_p \, dx \tag{17}$$

$$\dot{Q}_{0-2H} = 8\lambda_l \Delta T p_p \ln \frac{\delta_{t\,0-2H} + \delta_{ne}\sqrt{2}}{\delta_{ne}\sqrt{2}} \tag{18}$$

In the above dependence δ_{ne} is the film thickness at which no more evaporation takes place and $\Delta T = T_{bs} - T_{sat}$. It can be expressed as [4,5]:

$$\delta_{ne} = \left(\frac{C_{Ham} T_{sat}}{\rho_l i_{lv} \Delta T}\right)^{1/3} \tag{19}$$

The Hamaker constant C_{Ham} can be calculated from the Lifshitz theory [11]. The value for copper interacting across water is $3 \ldots 4 \cdot 10^{-19}$ J [11]. The value of C_{Ham} for R-123 was adopted after Chien and Webb as equal to $2 \cdot 10^{-12}$ J [4]. The difference between the local (tunnel) saturation temperature and the bulk saturation temperature was neglected, i.e.: $T_{sat,tun} \approx T_{sat}$. Referring the latent heat transfer rate from Eq. (18) to total surface area inside tunnels and to the area limited by the segment pitch (for pore pitch p_p—Fig. 5), we obtain the expression for the tunnel heat flux for the active pore:

$$q_{tun\,H} = \frac{\dot{Q}_{0-2H}}{2p_p(w_{tun} + h_{tun})} \tag{20}$$

4.4. Bubble frequency and nucleation site density

The waiting period was determined based on latent heat transfer inside the segment of the horizontal tunnel:

$$\int_0^{t_{1H}} \dot{Q}_{0-1\,H}\, dt = i_{lv} \Delta V_{l\,0-1\,H} \rho_l \tag{21}$$

Applying Eq. (7) for change of the liquid volume during phase 0–1, we obtain the expression for the waiting period:

$$\Delta t_{0-1H} = \frac{i_{lv}\rho_l \Delta V_{l\,0-1\,H}}{\dot{Q}_{0-1H}} \tag{22}$$

The tunnel heat transfer rate for the waiting period was calculated from Eq. (18) by replacing $\delta_{t\,0-2\,H}$ with the dependence for the height of the equivalent triangular section as the mean value for the whole period (0–1):

$$\delta_{t\,0-1\,H} = \sqrt{\frac{V_{l0\,H} + V_{l1H}}{8p_p}} \tag{23}$$

Found in literature dependences for the bubble radius change in the function of time in the growth period are usually the extensions of the Rayleigh equation, for instance as in [12]:

$$R_{1-2}\frac{d^2R_{1-2}}{dt^2} + \frac{3}{2}\left(\frac{dR_{1-2}}{dt}\right)^2 = \frac{1}{\rho_l}\left(p_v - p_l - \frac{2\sigma}{R_{1-2}}\right) \tag{24}$$

The equation refers to the case in which the growth rate is controlled by inertia forces. Chien and Webb [4] presented a modification of the transformed equation (24) through the separation of superheat ΔT and introduction of experimental constant C_{tg}, so that a different mechanism of bubble growth for a tunnel structure could be considered. The growth period was determined based on the dependence [4]:

$$\Delta t_{1-2\,H} = \frac{1}{C_{tg}}\left[\frac{7}{\pi}\frac{\rho_l T_{sat}}{i_{lv}\rho_{v1}\Delta T}\frac{(d_{bH}+d_p)}{(d_{bH}-d_p)}\right]^{1/2}\left(\frac{d_{bH}-d_p}{2}\right) \tag{25}$$

C_{tg} is a dimensionless empirical constant equal to 0.0296 [4,5]. The bubble departure diameter d_{bH} was calculated from Eq. (9). Numerical simulations proved the suitability of this formula in relation to the considered surfaces of horizontal tunnels. Other authors [5,13] also used this dependence for calculating the waiting period for flat surfaces.

Apart from the liquid intake period, the bubble departure frequency can be calculated as an inverse of the sum of the waiting and the growth periods, obtained from Eqs. (22) and (25):

$$f_H = \frac{1}{\Delta t_{0-1\,H} + \Delta t_{1-2\,H}} \tag{26}$$

For the calculated from Eq. (20) tunnel heat flux, with heat balance for the active pores, the nucleation site density for the horizontal tunnel can be expressed as:

$$n_{sH} = \frac{q_{tun\,H}}{\rho_{vm} i_{lv} f_H \frac{\pi d_{bH}^3}{6}} \tag{27}$$

The multiplication of both sides of the above equation (27) by the reference surface, for instance of one horizontal tunnel (cross section area $= sp_{tun}$), gives the number of active pores (N_a) for the considered surface. Non-active segments will contribute to the lowering of $q_{tun\,H}$ to the value of $q_{tun\,H}(N_a/N_{max}) = q_{tun\,H}(n_{sH}/n_{sH\,max})$ where, for the considered surface, N_{max} and $n_{sH\,max}$ denote the maximum number of pores and the maximum density of nucleation sites respectively. For instance, with $\Delta T = 2.3$ K, for the surface 10–2.50–0.3, $n_{sH}/n_{sH\,max} = 0.25$, that is in one horizontal tunnel (reference surface 2.5 mm × 5 mm) two pores out of total 8 are active. Increasing superheat to 17.2 K makes $n_{sH}/n_{sH\,max}$ reach the value 0.73, so we may assume that during the increase in ΔT four more pores were activated. All the data for water and R-123 are presented in Fig. 14.

Since the growth in bubble departure frequency is smaller than the growth in $q_{tun\,H}$ while increasing the superheat, the nucleation site density calculated from Eq. (27) will grow with the increase in ΔT (Fig. 11).

4.5. External and total heat flux

Haider and Webb formulation [2,4,5] of the total external heat flux assumes that the final part of the bubble cycle is dominated by micro-convection. Due to significant overestimation of the convection heat flux for horizontal tunnel calculated from Haider and Webb formula, the dependence of Mikic and Rohsenow [3] was used:

$$q_{ex\,H} = 2\sqrt{\pi \lambda_l \rho_l c_p f_H} d_{bH}^2 n_{sH} \Delta T \tag{28}$$

where ΔT is the wall superheat related to the horizontal perforated foil level.

Microconvection above the horizontal tunnel is limited by an intensive liquid flow towards holes in the vertical foils. Therefore, after [3], it was assumed in Eq. (28) that "the main mechanism of heat transfer in nucleate boiling is transient heat conduction to the liquid superheated layer around boiling sites". The advantage of Eq. (28) is the absence of experimental constants.

The total heat flux for horizontal tunnel, with the active pores to overall number of pores ratio can be calculated from the dependence:

$$q_H = q_{\text{tun}\,H}\frac{N_a}{N_{\max}}\frac{w_{\text{tun}}}{p_{\text{tun}}} + q_{\text{ex}\,H} \tag{29}$$

Finally, since $N_a/N_{\max} = n_{sH}/n_{sH\,\max}$ and $n_{sH\,\max} = 1/(p_p p_{\text{tun}})$ the total heat flux for horizontal tunnel becomes:

$$q_H = q_{\text{tun}\,H} n_{sH} p_p w_{\text{tun}} + q_{\text{ex}\,H} \tag{30}$$

5. Vertical tunnel modeling

Due to the temperature change along the height of the vertical fin (and the vertical tunnel at the same time), the calculations were conducted for the vertical tunnel total volume, that is $V_{\text{tun}\,V} = w_{\text{tun}} h_{\text{tun}} h_f$, Fig. 7. Unlike the horizontal tunnel with a steady temperature, it was not possible to analyze a separated segment of p_p dimension. External heat flux was related to the main fins bases.

5.1. Vapor density

Considering the fact that vapor bubbles get out only through open outlets of vertical tunnels, their hydraulic diameter was calculated with the following formula:

$$d_h = \frac{2 w_{\text{tun}} h_{\text{tun}}}{w_{\text{tun}} + h_{\text{tun}}} \tag{31}$$

When pores diameters d_p were replaced by hydraulic diameter d_h, vapor density at the end of the waiting and growth period could be calculated from Eq. (3). In the case of the vertical tunnel, vapor gets out only through the tunnels outlets at the main fins tips (with a hydraulic diameter of d_h); in a horizontal tunnel—through the pores. Vapor density defined by Eq. (3) depends on the diameter of the hole that "releases" the vapor (with other parameters unchanged), so by using d_h instead of d_p the end-of-the waiting-period density was obtained. At the tip of a fin the wall superheat is always sufficient to initiate and sustain nucleate boiling—vapor condensation is not possible in the upper regions of the vertical channels.

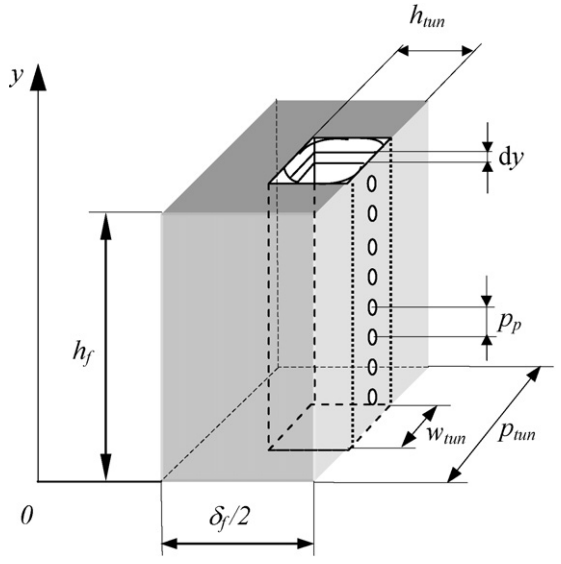

Fig. 7. A vertical tunnel referred to the segment volume $h_f \times \delta_f/2 \times p_{\text{tun}}$.

5.2. Liquid volume

Replacing a pore diameter by a hydraulic diameter in Eq. (9), one can calculate the diameter of a departing bubble at the vertical tunnel outlet d_{bV}, for $Bo = [d_h^2(\rho_l - \rho_v)g]/\sigma$. Analogically, adding the vertical tunnel volume in the form of $V_{\text{tun}\,V} = w_{\text{tun}} h_{\text{tun}} h_f$, we use Eqs. (7), (8), (13), (14) for calculating the liquid volume changes in vertical menisci of the tunnel and a liquid volume in menisci at the beginning of the waiting period (0), at the end of the waiting period (1) and the growth period (2).

5.3. Vertical tunnel heat flux

With Eq. (17) and the assumed temperature change at the main fin height ($0 \leqslant y \leqslant h_f$) as $\Theta = \Delta T \mathrm{e}^{-m_f y}$, where Θ denotes local temperature superheat in the fin vertical section, the dependence for the latent heat transfer rate from four menisci of vertical tunnel during waiting and growth periods takes the form, Fig. 7:

$$\dot{Q}_{0\text{–}2\,V} = 8\lambda_l \Delta T \ln\frac{\delta_{t\,0\text{–}2\,V} + \delta_{\text{ne}}\sqrt{2}}{\delta_{\text{ne}}\sqrt{2}} \int_0^{h_f+\delta_f/2} \mathrm{e}^{-m_f y}\,\mathrm{d}y \tag{32}$$

The necessity to simplify numerical calculations entailed the adoption of the approximate temperature distribution according to the dependence for the infinitely long fin $\Theta = \Delta T \mathrm{e}^{-m_f y}$. It is in accord with the assumption that the temperature at the fin tip approaches the ambient temperature, that is, the temperature of the boiling liquid.

Literature, e.g. [14], suggests that $m_f h_f \geqslant 3$ is sufficient for the infinite fin approximation in computing the heat transfer between the fin and the surroundings. This assumption is satisfied in the boiling of water on the considered surfaces after the implementation of the corrected height formula. Moreover, the temperature distribution measurements and theoretical analysis presented in [15] show that for the fin with TS the temperature at its tip is close to the water saturation temperature for the heat fluxes from 65 kW/m^2 up to 587 kW/m^2. It justifies the use of the simplified solution to the temperature distribution for this case.

The corrected height formula ($h_f + \delta_f/2$) was used as a substitute for the effect of heat transfer through the fin tip.

The height of the equivalent triangular cross-section $\delta_{t\,0\text{–}2\,V}$ was calculated by:

$$\delta_{t\,0\text{–}2\,V} = \sqrt{\frac{V_{l0V} + V_{l2V}}{8h_f}} \tag{33}$$

For the sake of simplicity it was assumed that the thickness of the non-evaporating liquid layer δ_{ne}, Figs. 4, 6, is constant at the height of the main fin. The integration of Eq. (32) results in the dependence:

$$\dot{Q}_{0\text{–}2\,V} = \frac{8\lambda_l}{m_f}\Delta T \ln \frac{\delta_{t\,0\text{–}2\,V} + \delta_{\mathrm{ne}}\sqrt{2}}{\delta_{\mathrm{ne}}\sqrt{2}}\left(1 - \mathrm{e}^{-m_f(h_f+\delta_f/2)}\right) \tag{34}$$

In order to accurately determine fin parameter m_f, it is necessary to consider the variable local heat transfer coefficient along the fin, which is specified by the dependence: $\alpha = A\Theta^n$. The same two constants A and n appear in the expression for heat flux $q = A\Delta T^{n+1}$, which means that it is necessary to know the boiling curve shape $q = q(\Delta T)$ to be able to determine them.

Due to the fact that the boiling curve is not known, exponent n can be calculated in two ways:

1. based on the correlation for TS, given in [16], then $n = 0.27$,
2. based on the dependence for the horizontal tunnel total heat flux (Eq. (30)) in the power form, that is: $q_H = A\Delta T^{n+1}$, then $n = 0.77$.

A small value of exponent n proves weak dependence of heat transfer coefficient on wall superheat, which means little change in α along the fin height (i.e. vertical tunnel). Thus the introduction of the mean heat transfer coefficient to the calculations is justified.

The mean heat transfer coefficient at the main fin height is determined according to the following dependence:

$$\alpha_m = \frac{1}{h_f}\int_0^{h_f+\delta_f/2} \alpha(y)\,\mathrm{d}y \tag{35}$$

The dependence for the local value of the heat transfer coefficient is expressed by:

$$\alpha(y) = A\left(\Delta T \mathrm{e}^{-m_f y}\right)^n \tag{36}$$

Constant A was calculated from the dependence:

$$A = \frac{q_H}{\Delta T^{n+1}} \tag{37}$$

Total heat flux for horizontal tunnel q_H was given by Eq. (30).

It was assumed that the temperature at the base of the vertical tunnel (coordinate $y = 0$, Fig. 7) is the same as the temperature of the horizontal tunnel, referred to the level of the perforated foil (coordinate $y = h_{\mathrm{tun}}$, Fig. 5). One can also assume that the superheat ΔT defined in this plane for the walls of the horizontal and vertical tunnels will be equal, due to the smooth "passing" from the horizontal to vertical tunnel, $\Delta T = \Theta(y = 0)$. The local heat flux for the vertical tunnel increases while approaching the main fin base. Hence, for $y = 0$, Fig. 7, it will be close to q_H defined for the horizontal tunnel since $q(y = 0) = A\Delta T^{n+1}$. In other words, temperatures and heat fluxes were assumed to be equal at the contact point of the horizontal and vertical tunnel walls, which makes it possible to determine the local value of the heat transfer coefficient for $y = 0$ (Fig. 7) in a simple way, having earlier calculated (Eq. (30)) the value of q_H. Substituting Eq. (37) for Eq. (36) and assuming that $y = 0$, we obtain the dependence for the local heat transfer coefficient at the base of the vertical fin: $\alpha_{\mathrm{bs}} = \alpha(y = 0) = q_H/\Delta T$.

Implementing Eq. (36) to Eq. (35) and integrating it makes the dependence for the mean heat transfer coefficient take the following form:

$$\alpha_m = \frac{A\Delta T^n}{m_{fm}nh_f}\left(1 - \mathrm{e}^{-m_{fm}n(h_f+\delta_f/2)}\right) \tag{38}$$

Parameter $m_{f\,\mathrm{bs}}$ was adopted as the first approximation of parameter m_{fm}, referred to the main fin base and calculated from the dependence:

$$m_{f\,\mathrm{bs}} = \sqrt{\frac{2\alpha_{\mathrm{bs}}(\delta_f + w_f)}{\lambda_m \delta_f w_f}} \tag{39}$$

In the above equation $\alpha_{bs} = q_H/\Delta T$, $2(\delta_f + w_f)$ denotes the main fin circumference, $\delta_f w_f$—cross-section area. An accurate calculation of the mean parameter m_{fm} is possible through the successive approximation method and adoption of the fin parameter according to the dependence:

$$m_{fm} = \sqrt{\frac{2\alpha_m(\delta_f + w_f)}{\lambda_m \delta_f w_f}} \tag{40}$$

The mean thermal conductivity of a fin was calculated for the segment with section $\delta_f/2 \times p_{\mathrm{tun}}$, Fig. 7. With the assumption that the tunnel is fully filled with vapor, we obtain:

$$\lambda_m = \frac{\lambda_v h_{\mathrm{tun}} w_{\mathrm{tun}} + \lambda_{\mathrm{Cu}}(p_{\mathrm{tun}}\delta_f/2 - h_{\mathrm{tun}} w_{\mathrm{tun}})}{p_{\mathrm{tun}}\delta_f/2} \tag{41}$$

When we assume that the tunnel is fully filled with boiling liquid, the change in the mean heat transfer coefficient will not exceed 0.12%.

The course of calculations for determining the mean value of parameter m_{fm}:

Input data: $h_{\mathrm{tun}}, w_{\mathrm{tun}}, p_{\mathrm{tun}}, w_f, \delta_{f,}, \lambda_v, \lambda_{Cu}, q_H, \Delta T$.

1. The heat transfer coefficient at the fin base is calculated from $\alpha_{bs} = q_H/\Delta T$.
2. The mean thermal conductivity is calculated from Eq. (41).
3. Parameter $m_{f\,\mathrm{bs}}$ is determined from Eq. (39).
4. The value of the exponent n and computing constant A are adopted from Eq. (37).
5. $m_{fm} = m_{f\,\mathrm{bs}}$ are substituted and α_m is calculated from Eq. (38).
6. Parameter m_{fm} is determined from Eq. (40).

Satisfactory accuracy is obtained already for the second approximation of m_{fm}, calculated from Eq. (40) (relative difference in values of successive approximations below 1%).

The vertical tunnel heat flux is given by:

$$q_{\mathrm{tun}V} = \frac{\dot{Q}_{0\text{–}2\,V}}{2h_f(w_{\mathrm{tun}} + h_{\mathrm{tun}})} \tag{42}$$

5.4. Bubble frequency and nucleation site density

According to the assumptions made earlier, evaporation of liquid takes place in all tunnels for the whole range of wall superheat. Thus the nucleation sites density remains constant and can be expressed as:

$$n_{sV} = \frac{2}{p_{\mathrm{tun}}(\delta_f + 2h_f)} \tag{43}$$

The frequency of the bubbles departure from the vertical tunnel outlet is defined by the dependence:

$$f_V = \frac{q_{\mathrm{tun}V}}{\rho_{vm} i_{lv} n_{sV} \frac{\pi d_{bV}^3}{6}} \tag{44}$$

Bubble departure diameter d_{bV} was calculated in the same way as for the horizontal tunnel, Eq. (9), with the use of hydraulic diameter given by Eq. (31).

5.5. External and total heat flux

In order to calculate the external heat flux, a modified Haider and Webb dependence [2] was used:

$$q_{\mathrm{ex}\,V} = 2\sqrt{\pi \lambda_l \rho_l c_p f_V} d_{bV}^2 n_{sV} \Delta T C_{\mathrm{conv}} \tag{45}$$

Initially, Haider and Webb, as well as Chien and Webb proposed the following dependence for convection term:

$$C_{\mathrm{conv}} = \left[1 + \left(\frac{0.66\pi c}{Pr^{1/6}}\right)^l\right]^{1/l} \tag{46}$$

They suggested the value of 6.42 for constant c and 2 for l in the above equation, whereas Ramaswamy et al. proposed a third order polynomial function of wall superheat for calculating constant c. This makes it necessary to use additional four experimental constants.

In order not to make the model more complicated, the dependence with only one empirical constant was proposed: $C_{\mathrm{conv}} = Pr^k$. Then, dependence (45) obtains the following form:

$$q_{\mathrm{ex}\,V} = 2\sqrt{\pi \lambda_l \rho_l c_p f_V} d_{bV}^2 n_{sV} \Theta_{\mathrm{tip}} Pr^k \tag{47}$$

The best agreement of the experimental data with the equation above, for $n = 0.27$ in the dependence $\alpha = A\Theta^n$, was achieved at $k = 4.9$ for water and $k = 1.42$ for R-123. When a different value of n is used, the corrected Prandtl number exponent for the water can be calculated from the approximated dependence $k = 5.5 - 2.2n$ (for n in $0.2 < n < 0.8$), with similar accuracy. For boiling refrigerant R-123, changes of exponent n do not entail the correction of k. Superheat at main fin tip Θ_{tip}, that is superheat at bubble departure site, can be calculated with the following well-known dependence for fin with insulated tip. Corrected fin height was applied as a substitute for the effect of heat transfer through the tip:

$$\Theta_{\mathrm{tip}} = \frac{\Delta T}{\cosh[m_{fm}(h_f + \frac{\delta_f}{2})]} \tag{48}$$

The dependence presented above considers the mean value of fin parameter m_{fm}, derived from formula (40). There might be a strong convective heat transfer from the vertical wall due to upstreaming bubbles from the horizontal tunnel. Therefore, the proposed modified Haider–Webb formula, Eq. (47) may work better than Mikic–Rohsenow dependence, Eq. (28), used for horizontal tunnel external heat flux calculation.

The total heat flux for the vertical tunnel is given by:

$$q_V = q_{\mathrm{tun}\,V}\frac{w_{\mathrm{tun}}}{p_{\mathrm{tun}}} + q_{\mathrm{ex}\,V} \tag{49}$$

The total heat flux for a system of connected horizontal and vertical tunnels, with the assumption that the space width between main fins is equal to their thickness, i.e. $s = \delta_f$ is expressed by the following equation:

$$q = \frac{q_H + q_V}{2} \tag{50}$$

6. Results of the model

Figs. 8 and 9 show exemplary experimental boiling curves for structures with a fixed pitch and variable pore diameters [16]. The best results for TS at high heat fluxes ($q > 100\ \mathrm{kW/m^2}$) were obtained for 0.4 mm pore diameter.

When compared to the smooth fin surface (3-fin array, 10 mm in height and 5 mm in thickness), the heat flux almost tripled for 10 K superheating, Fig. 8. Also the heat transfer coefficient was almost 3 times greater for 100 $\mathrm{kW/m^2}$ heat flux [16], Fig. 9. For low heat fluxes, all tested TS gave similar values of the heat transfer coefficient. These structures revealed almost constant value of the coefficient (about 30 $\mathrm{kW/m^2\,K}$) in the 100–500 $\mathrm{kW/m^2}$ heat flux range. For the three boiling curves presented in Fig. 8 the mean exponent n is 0.21 (so $q \propto \Delta T^{1.21}$ because $q = A\Delta T^{n+1}$). It agrees with the smaller value of the proposed exponent n (0.27) in the dependence for the heat transfer coefficient, $\alpha = A\Theta^n$. This proves that the earlier statement relating to small changes in q and α in the function

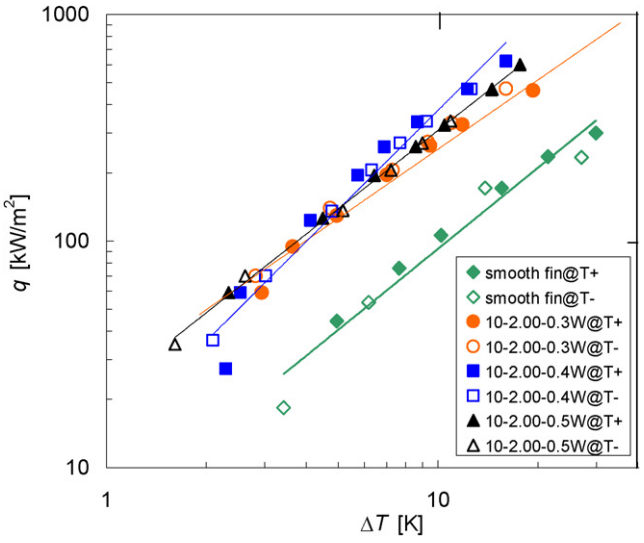

Fig. 8. Effect of pore diameter on the boiling of water, mini-fin pitch 2.00 mm, $T+$—superheat increasing, $T-$—superheat decreasing.

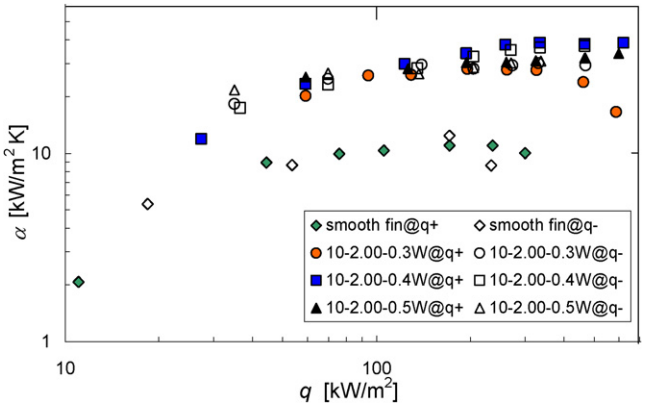

Fig. 9. Effect of pore diameter on the boiling of water, mini-fin pitch 2.00 mm, $q+$—heat flux increasing, $q-$—heat flux decreasing [16].

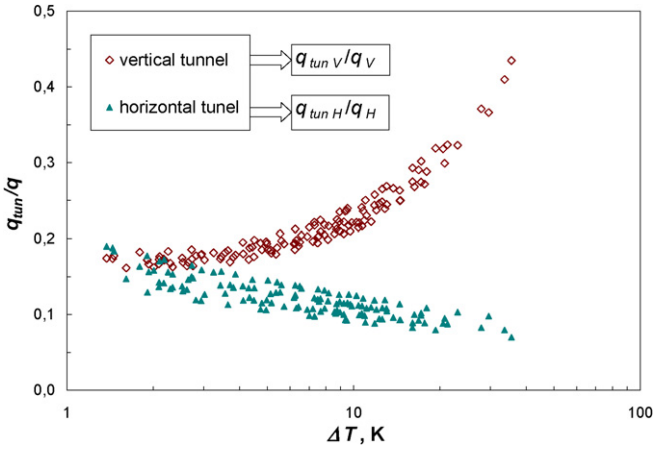

Fig. 10. Calculated tunnel to total heat flux ratio for the horizontal and vertical tunnel referred to the temperature superheat in the boiling of water.

of superheat was correct. In reference to the chart in Fig. 9 data may be fit with expression $\alpha \propto q^{0.17}$. Publications on nucleate pool boiling correlations usually give dependences with much bigger exponent values, i.e., $q \propto \Delta T^3, \alpha \propto \Delta T^2, \alpha \propto q^{0.7}$ [12].

Fig. 10 refers exclusively to the comparison of the evaporation heat flux to total heat flux ratio for the horizontal tunnel and the evaporation heat flux to total heat flux ratio for the vertical tunnel. The evaporation heat flux to total heat flux ratio for the horizontal tunnel shows a slight fall from about 0.2 to 0.1–0.15 with the increased temperature superheat, Fig. 10. The mean value of this ratio for the vertical tunnel was increasing from 0.15–0.2 to 0.45, which may result from the adopted differences in boiling modeling in relation to those two types of tunnels. This denotes the determinative contribution of external heat flux for the horizontal tunnel. Vertical tunnels have an inverse course of change and the tendency to balance the contributions of tunnel and external heat fluxes at increasing superheat is their characteristic feature.

For instance, at 20 K wall superheat $q_{\mathrm{tun}\,V}/q_V \approx 0.3$ and $q_{\mathrm{tun}\,H}/q_H \approx 0.1$. It means that the contribution of evaporation heat flux, in reference to the total heat flux transferred from the vertical tunnel, is three times bigger than the analogical contribution referred to the horizontal tunnel. The data have no reference to Fig. 13 that shows the ratio of the vertical tunnel total heat flux ($q_V = q_{\mathrm{tun}\,V} + q_{\mathrm{ez}\,V}$) to horizontal tunnel total heat flux ($q_H = q_{\mathrm{tun}\,H} + q_{\mathrm{ex}\,H}$). For the given superheat, $q_V/q_H \approx 0.15$ (Fig. 13).

A comparison of the experimentally observed values and the predicted values for bubble departure frequency in a horizontal and vertical tunnel is shown in Fig. 11. In the case of the horizontal tunnel (Fig. 11a), the authors used experimental data by Chien and Webb [17,18], related to the boiling of R-123 in tunnels with pores of 0.23 mm in diameter. Calculations based on our own model were carried out for 0.3 and 0.23 mm pore diameters. For pores with diameters of 0.23 mm high agreement with Chien–Webb experimental data was obtained (maximum error in comparison to the experimental data is not bigger than 15%). The experimental data for the vertical tunnel (Fig. 11b) were obtained by means of high-speed photography (193 fps): for each superheat 5 frequency measurements referred to three randomly chosen tunnel outlets were taken and averaged. The measurements showed satisfactory agreement with the theoretical calculations. The maximum error of computed frequencies, compared to the experimental data, do not exceed 30% and occur for small superheats, 2–3 K. This may be a result of the fact that the model predicts permanent activity of all the vertical tunnels outlets, whereas the observations helped to notice that at small superheats not all the outlets of the tunnels were active.

Fig. 12 shows the comparison of the measured diameters of departing bubbles for selected surfaces in the boiling of water and R-123, and the values computed according to dependence (9). The discrepancy between the measurements and calculations reaches 15% for water and 30% for R-123. The measurements were based on the photographs from a digital camera. The estimated error in defining the diameter was up to 10% (including the error resulting from the non-sphericity of bubbles). A little increase in the diameter for superheats of 4–5 K is quite characteristic, but insufficient amount of measurement data prevents drawing any general conclusions.

Fig. 13 presents the ratio of total heat flux for the vertical tunnel to total heat flux for the horizontal tunnel. It seems that boiling heat transfer in vertical tunnels has the dominant contribution to the total heat transfer enhancement for the boiling of R-123. It is especially visible at small superheats ($q_V/q_H \approx 20$ at $\Delta T \approx 2$ K). At larger ΔT the heat transfer contribution in horizontal tunnels increases ($q_V/q_H \approx 5$). For the boiling of water, at superheats of about 4 K, the contribution of vertical and horizontal tunnels to the total heat transfer becomes balanced. At superheats of $\Delta T > 4$ K (which corresponds to experimental heat flux about 100 kW/m^2) the horizontal tunnel is dominant. These facts result from the constant activity of all the vertical tunnels and gradual activation of pores in inter-fin spaces. This means that constant density of nucleation sites is retained with increasing superheat in vertical tunnels; in horizontal tunnels a significant increase in n_s, takes place, especially in the boiling of water (Fig. 14). This results in the decrease of the vertical tunnel heat flux with increasing wall superheat (Fig. 13). For small superheats ΔT at the main fin base, the superheat of the walls at the tunnel outlets is close to zero,

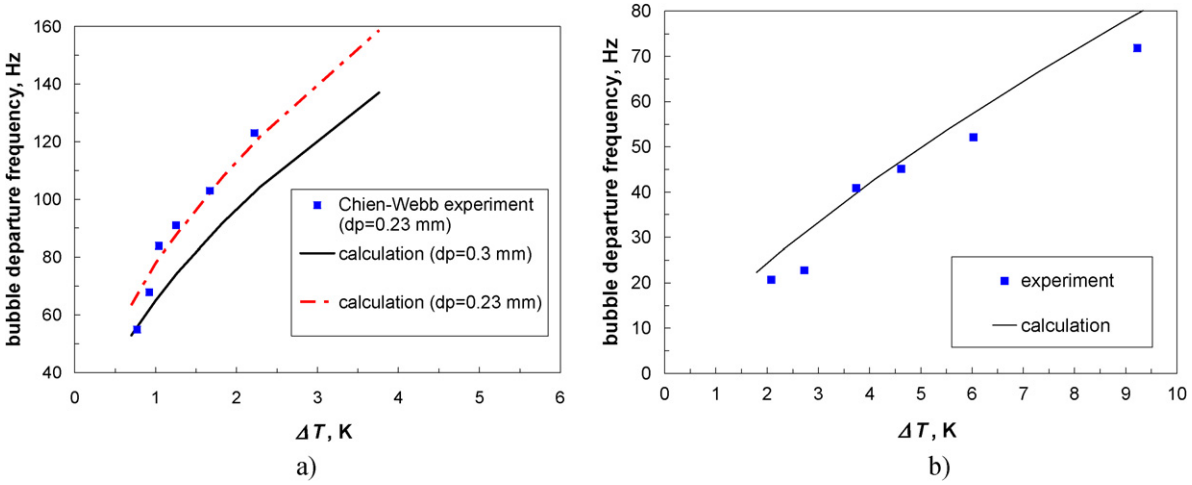

Fig. 11. Comparison of the calculated and measured departure bubble frequency: a) for the horizontal tunnel at R-123 boiling (experimental data from Chien–Webb [17,18] for pore diameter 0.23 mm); b) for the vertical tunnel at the boiling of water (experimental data for sample TS-10-2.50-0.3).

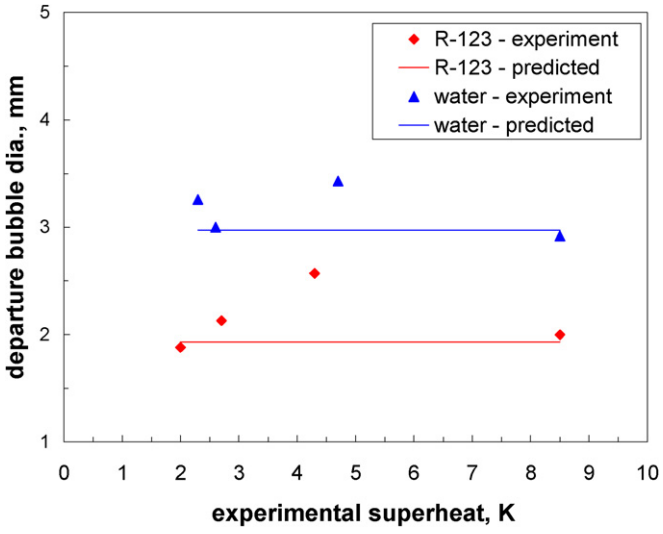

Fig. 12. The measured departure bubble diameter for the vertical tunnel ($d_h = 1.43$ mm) in comparison with the prediction (water boiling—sample TS-10-2.00-0.3, R-123 boiling—sample TS-10-2.50-0.5).

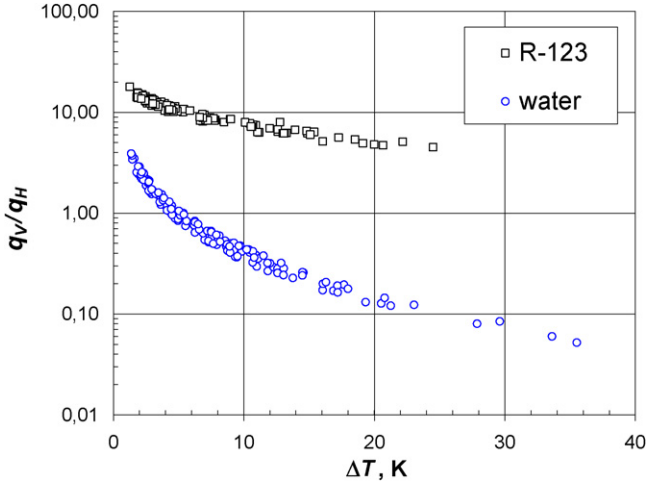

Fig. 13. Calculated vertical to horizontal tunnel total heat flux ratio.

that is, why vapor generation, resulting from the evaporation from menisci, takes place only in the lower parts of vertical tunnels. The bubbles move upwards inside the tunnel towards its outlet, and their place is taken by next portions of evaporating liquid. The results of the internal visualization, described in [8] can prove this reasoning: vapor volumes in the tunnels were separated by liquid layers.

Additional explanation to these phenomena might be the fact that vapor, which is originally generated in the horizontal tunnels due to higher local wall superheat, flows into the vertical tunnels. This might be caused by lower hydraulic resistance at the connection of vertical and horizontal tunnels (hydraulic diameter about 1 mm) in comparison to the higher capillary resistance at the pores with diameter of 0.3–0.5 mm.

The observation of the boiling process, as well as the adopted assumptions concerning the horizontal tunnel allow us to conclude that up to certain superheats, corresponding to the bubble coalescence initiation, an active pore has to adjoin at least one inactive pore. In this way the active segment is effectively supplied with liquid. For water the superheat was then about 10 K, $q \approx 300$ kW/m^2 and $n_{sH}/n_{sH\,\max} \approx 0.5$ (Fig. 14). Thus the density of nucleation sites should be smaller than the maximum theoretical density obtained when all the pores are activated (see formula (29)). As shown in graph (Fig. 14), nucleation sites density increases as a power function. For the boiling of water only at maximum superheats the ratio $n_{sH}/n_{sH\,\max}$ exceeds the value of 0.75, which leads to tunnel dry-out. Only few data exceeded this value.

The nucleation site density for water at 20 K wall superheat is approx. 70% (Fig. 14). In Fig. 9 the heat transfer coefficient for the corresponding heat flux of 500 kW/m^2 is constant or decreasing. This indicates the region of critical heat flux where vapor blocks the channels. On some of the investigated surfaces, however, nearly all pores are activated at maximum superheat. The fact that for most these surfaces the $n_{sH}/n_{sH\,\max}$ ratio does not exceed 0.75 can mean that some of the pores in the horizontal tunnel can remain inactive along the whole cycle of increasing heat flux. Their sole role is to supply liquid

into the active segment. This does not question the assumption about independent "work" of each segment during the waiting and growth periods—the assumptions do not specify the way the liquid is supplied in the intake period, that is the liquid can flow in either through the active segment pore, or through the tunnel from the adjacent, non-active segment. Due to the significant demand for liquid at large superheats, the segments of non-active pores will have a function of an exclusive liquid supply for neighboring active segments. This explanation can confirm the calculations performed for the boiling agent R-123 (Fig. 14)—at the largest superheats ($\Delta T \approx 25$ K) about 80% of horizontal tunnels segments remain non-active.

Furthermore, when bubbles from active pores join at large superheats, they may induce the blockage of non-active (supplying) pores which in turn will cause the dry-out of horizontal tunnels. The coalescence of bubbles departing from horizontal tunnels contributes to both the intensification of this phenomenon and blockage of liquid supply for pores in vertical tunnels. The joint effect of the described phenomena includes the dry-out of both tunnels and the approaching boiling crisis.

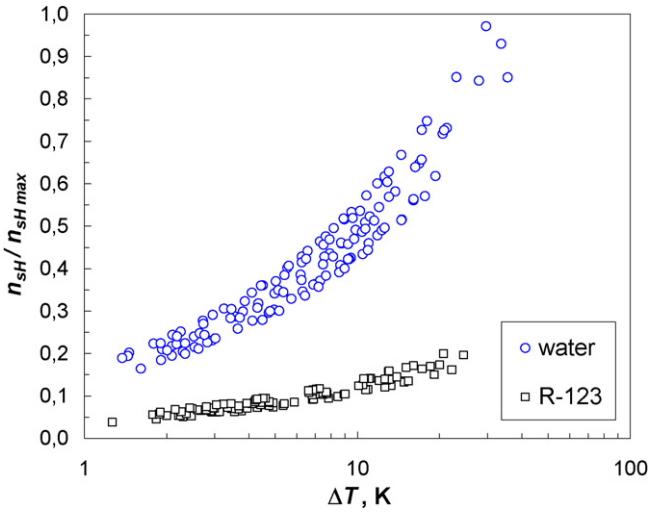

Fig. 14. Nucleation site density to theoretical maximum nucleation site density ratio for horizontal tunnel (model computation).

In the boiling of R-123 calculation results show much smaller densities of nucleation sites ($n_{sH}/n_{sH\,\max} < 0.2$), which prevents coalescence at maximum superheats and ensures better accuracy of modeling in accordance with the adopted simplifying assumptions (Fig. 16).

Fig. 15 presents the comparison of experimental data for water with the values of q calculated from Eq. (50) for exponent $k = 4.9$, and for structures given in Table 1.

The proposed semi-analytical approach helps calculate the boiling heat flux which agrees (with ±40% tolerance) with the measurements for about 87% of data for water and below 300 kW/m^2—for 95% of data. For heat fluxes above 300 kW/m^2 the approach does not reflect the deviation towards a constant heat flux value, when the discrepancies may reach 300%. Similar deviation of some data from the predicted ones was noticed by Nakayama et al. [1] for higher heat fluxes, for R-11 and liquid nitrogen. The causes of the observed facts were not given.

This phenomenon in the present model can be explained by the following facts:

- The model refers to the *isolated bubble regime* and for $q >$ 300 kW/m^2, due to bubble coalescence, it is encumbered with an error that increases with increasing heat flux,
- Intensified vapor production inside the horizontal tunnel at high values of wall superheat and heat flux can disturb supplying the vertical tunnel with liquid. This results in the lowering of departing bubbles frequency at the vertical tunnel outlet.
- Assumptions included spherical shape and a constant diameter of the vapor bubbles. In fact, there are deformations of the assumed spherical shape.
- Horizontal and vertical tunnels were assumed to work independently owing to different directions of liquid inflow.

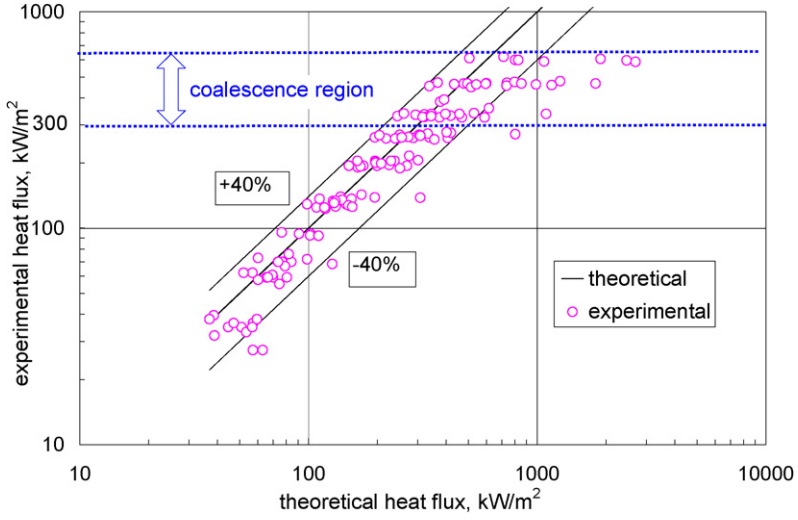

Fig. 15. A comparison of experimental and theoretical heat fluxes for the boiling of water, $k = 4.9$ in Eq. (47).

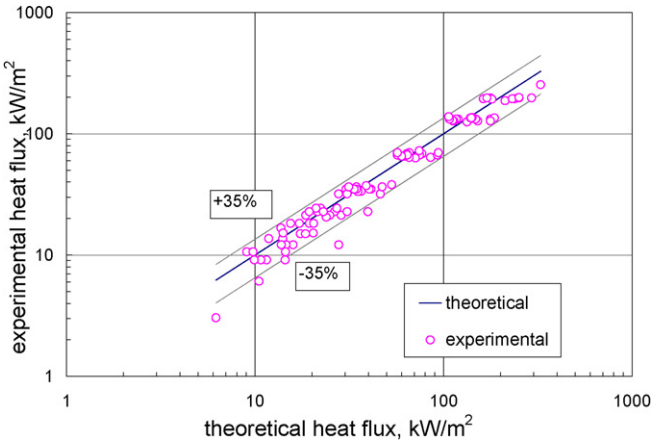

Fig. 16. Comparison of experimental and theoretical heat fluxes for the boiling of R-123, $k = 1.42$ in Eq. (47).

Far better results were obtained when the proposed semi-analytical approach was used with respect to the boiling coolant R-123. Nearly 96% of the experimental data for R-123 were predicted fairly accurately, that is with maximum error of ±35%, Fig. 16. Also for the top values of heat fluxes, below the boiling crisis (about 200 kW/m^2), the calculated values were congruent with experimental values in the specified above range of error. A small contribution of horizontal tunnels in the overall heat transfer is caused by smaller nucleation sites densities, which are a few times smaller that those for water boiling (Fig. 14), which in turn weakens the tendency of bubbles to join.

7. Final remarks and conclusions

The presented model makes it possible to determine the departure diameter, frequency and total heat flux both for horizontal and vertical subsurface tunnels limited by thin porous foil. The input data were the following:

- geometrical dimensions of the tunnel and main fin (h_{tun}, w_{tun}, p_{tun}, h_f, $\delta_{f,}$, w_f);
- pore dimensions (d_p, p_p);
- boiling liquid and saturated vapor properties ($\rho_{v\,\text{sat}}$, $\rho_{l,}\sigma$, $\lambda_{v,}\lambda_l$, i_{lv}, $\mathbf{R}$, T_{sat});
- structure material thermal conductivity (λ_{Cu});
- Hamaker constant C_{Ham};
- Chien–Webb constant C_{tg} [1] used for the model of bubble growth period for the horizontal tunnel;
- superheat (ΔT) related to main fin base;
- exponent n in dependence for the value of the heat transfer coefficient $\alpha = C\Delta T^n$ (from correlation in [16] or based on dependence $q_H = A\Delta T^{n+1}$);
- experimental constant k in dependence for the external heat flux of the vertical tunnel.

The proposed model was based on the existing Haider–Webb, Chien–Webb, Ramaswamy et al., and Nakayama et al. models. The authors introduced a number of their own dependences. The most significant differences are the following:

- The authors' own analytical calculations of the evaporated liquid volumes in the waiting period and the waiting and growth period were presented. Also new dependences for the initial and final vapor volume in the tunnel, the liquid volumes in menisci for the beginning of the waiting period and the end of the growth period were obtained.
- In order to determine the heat flux in the meniscus, a simplified calculation was proposed: its real cross-section was replaced by a triangular section.
- The total heat flux for horizontal tunnel was calculated considering active to overall number of pores ratio.
- For vertical tunnels constant density of nucleation sites was assumed, which simplified the calculation of bubble departure frequency.
- Another assumption referred to the heat transfer coefficient change along the main fin height, in accordance with the dependence following from the boiling curves.
- In order to make the model less complicated, the authors proposed the dependence for vertical tunnel external heat flux, with only one empirical constant in the convection term.

The following dependences were taken from the existing models:

- the dependence for bubble departure diameter d_b was adopted after [4];
- the film thickness at which no more evaporation takes place adopted from [4,5];
- the value of C_{Ham} for R-123 was adopted according to [4];
- the growth period was determined based on the dependence [4].

Having made the corrections and having added experimental data for R-123, the authors obtained a substantial improvement in the accuracy of the model, with respect to the initial model presented in [9]. Especially for R-123, the accuracy is similar to that of Ramaswamy et al. [5] for FC-72.

The following main conclusions can thus be drawn:

(1) The use of the analyzed structures makes the heat transfer coefficients triple in value when compared with smooth fins in the boiling of water (Fig. 9), which, maintaining similar dimensions, is important in cooling electronic systems, processors, etc.
(2) Generally speaking, vertical tunnels are more influential at R-123 boiling heat transfer for the whole range of the used heat fluxes, whereas in the boiling of water—for small and medium heat fluxes used in the experiment.
(3) The adopted assumptions and simplifications helped build a semi-analytical model which provides a prediction of heat flux within ±40% for the boiling of water and ±35% for the boiling of R-123. High complexity of the considered structure, together with the adopted simplifying assumptions cause errors with respect to the presented in literature models for typical uniform surfaces. The proposed model gives satisfactory results for low and medium heat fluxes

for water (up to 300 kW/m^2) and for all range of heat fluxes for R-123 boiling.

(4) It turned out that the best results are obtained with the Mikic–Rohsenow dependence for calculating convection heat flux for a horizontal tunnel, and with the modified Haider–Webb dependence in relation to a vertical tunnel.

(5) The presented boiling model can be used for optimization analysis of the investigated subsurface structures, with the aim of selecting the structure parameters that ensure the highest heat transfer coefficients.

Acknowledgements

This paper was partially supported by The Polish Ministry of Education and Science, Grant No. 3T10B 06529.

References

[1] W. Nakayama, T. Daikoku, H. Kuwahara, T. Nakajima, Dynamic model on enhanced boiling heat transfer on porous surfaces. Part II—analytical modeling, ASME Journal of Heat Transfer 102 (1980) 451–456.

[2] S.I. Haider, R.L. Webb, A transient microconvection model of nucleate pool boiling, Int. Journal of Heat and Mass Transfer 40 (1997) 3675–3688.

[3] B.B. Mikic, W.M. Rohsenow, A new correlation of pool boiling data including the effect of heating surface characteristics, ASME Journal of Heat Transfer 91 (1969) 245–250.

[4] L.-H. Chien, R.L. Webb, A nucleate boiling model for structured enhanced surfaces, Int. Journal of Heat and Mass Transfer 41 (1998) 2183–2195.

[5] C. Ramaswamy, Y. Yoshi, W. Nakayama, W.B. Johnson, Semi-analytical model for boiling from enhanced structures, Int. Journal of Heat and Mass Transfer 46 (2003) 4257–4269.

[6] R. Pastuszko, M.E. Poniewski, P.J. Mroczek, Boiling heat transfer enhancement on fin arrays with extended micro-surfaces, in: Proc. 3rd Int. Symp. on Two-Phase Flow Modeling and Experimentation, 2004, Pisa, Italy, paper mt-12.

[7] R. Pastuszko, T.M. Wojcik, P.J. Mroczek, Boiling visualization on fins with tunnel structure, in: Proc. 10th Int. Symp. on Heat Transfer and Renewable Sources of Energy, Miedzyzdroje, Poland, 2004, pp. 621–628.

[8] R. Pastuszko, P.J. Mroczek, Boiling visualization for fins with horizontal and vertical subsurface tunnels, in: Proc. 11th Int. Symp. on Heat Transfer and Renewable Sources of Energy, Miedzyzdroje, Poland, 2006, pp. 629–636.

[9] R. Pastuszko, M.E. Poniewski, Boiling heat transfer on double-extended surfaces with joined horizontal and vertical tunnels, in: Proc. 6th Int. Conference on Boiling Heat Transfer, Spoleto, Italy, 2006, paper No. 54.

[10] Y. Chen, M. Groll, R. Mertz, A dynamic model for pool boiling heat transfer on enhanced surfaces with sub-surface channels, in: Proc. 3rd Int. Symp. on Two-Phase Flow Modeling and Experimentation, 2004, Pisa, Italy, paper No. pst01.

[11] J.N. Israelachvili, Intermolecular and Surface Forces, Academic Press, 1985.

[12] J.R. Thome, A. Bejan, A.D. Kraus (Eds.), Heat Transfer Handbook, John Wiley & Sons, Inc., 2003 (Chapter 9).

[13] A.K. Das, P.K. Das, S. Bhattacharyya, P. Saha, Nucleate boiling heat transfer from a structured surface—Effect of liquid intake, Int. Journal of Heat and Mass Transfer 50 (2007) 1577–1591.

[14] J.H. Lienhard IV, J.H. Lienhard V, A Heat Transfer Textbook, Phlogiston Press, Cambridge, MA, 2004.

[15] R. Pastuszko, Temperature distribution in fin with tunnel structure, in: Proc. 4th Int. Conf. on Transport Phenomena in Multiphase Systems HEAT 2005, Gdansk, Poland, 2005, pp. 421–426.

[16] R. Pastuszko, Boiling heat transfer on double-extended surfaces, in: Proc. 10th Int. Symp. on Heat Transfer and Renewable Sources of Energy, Miedzyzdroje, Poland, 2004, pp. 629–636.

[17] S. Murthy, Y. Joshi, S. Gurrum, W. Nakayama, Enhanced boiling heat transfer simulation from structured surfaces: Semi-analytical model, Int. Journal of Heat and Mass Transfer 49 (2006) 1885–1895.

[18] L.H. Chien, R.L. Webb, Measurement of bubble dynamics on an enhanced boiling surface, Experimental Thermal and Fluid Science 16 (1998) 177–186.